Unprecedented bi- and trinuclear palladium(II)-sodium complexes from a salophen-type Schiff base: Synthesis, characterization, thermal behavior, and in vitro biological activities

Atousa Goudarzi[a], Maryam Saeidifar[b], Kioumars Aghapoor[a], Farshid Mohsenzadeh[a], Dieter Fenske[c], Olaf Fuhr[c], Mitra Ghassemzadeh[a,*]

[a] *Department of Inorganic Chemistry, Chemistry & Chemical Engineering Research Center of Iran, Pajoohesh Blvd., 17th Km of Tehran–Karaj Highway, Tehran 14968-13151, Iran*
[b] *Department of Nanotechnology and Advanced Materials, Materials and Energy Research Center, Karaj, Iran*
[c] *Institut fuer Nanotechnologie (INT) and Karlsruhe Nano Micro Facility (KNMFi), Karlsruher Institut fuer Technologie (KIT), Hermann-von-Helmholtz-Platz 1, Eggenstein-Leopoldshafen 76344, Germany*

ARTICLE INFO

Keywords:
Ultra-fast sonochemical synthesis
Pd-Na and Pd-Na-Pd Schiff base complexes
Molecular structures
Antibacterial activity
Antitumor activity
Nanoscaled materials

ABSTRACT

Novel bi- and trinuclear palladium(II)-sodium complexes, {[P*d*L]Na(NO_3)(EtOH)} (**1**) and {[P*d*L]$_2$Na}Cl (**2**) based on salophen-type Schiff base N,N'-(1,2-phenylene)-bis(3-methoxysalicylideneimine) (H_2L) were synthesized under ambient and sonochemical conditions. Ultrasonication proved to be a more effective method for the rapid synthesis of these bi- and trinuclear complexes under mild conditions. On the basis of the molecular structure of complexes **1** and **2**, each palladium atom is placed in the "inner" N_2O_2 compartment, and the sodium atoms are located in the "outer" $O_2O'_2$ compartment of the twofold deprotonated *bis*-Schiff base ligand. In both complexes, each Pd(II) ion is four coordinated showing square planar geometry, whereas the Na(I) ions in complexes **1** and **2** adopt two different geometries, namely hepta and octa coordination, respectively. In addition, the solventless thermolysis of both complexes at 500 °C was also studied by thermal gravimetric analysis (TGA). EDX and powder XRD data pointed out the presence of highly pure nanoscaled materials. Furthermore, the anticancer and antibacterial activities of bi- and trinuclear complexes were examined towards MCF-7 human breast cancer cell line and evaluated against one gram-negative strain (*Escherichia coli* ATCC 25922) and one gram-positive strain (*Staphylococcus aureus* ATCC 6538). The in vitro studies revealed that complex **2** exhibited higher anticancer activity against MCF-7 cell line as well as better antibacterial effect on the examined bacteria strains than complex **1**.

1. Introduction

Schiff bases (SB) form a large group of organic compounds with at least one azomethine group ($R_1HC{=}N\text{-}R_2$) in their structure, which can be obtained from the condensation reaction of a primary amine with a compound containing a carbonyl functional group under various reaction conditions. Since their introduction for the first time by Hugo Schiff in 1864 [1,2], it has been suggested that the donor property of iminic nitrogen atom as a Lewis base (presence of lone pair electrons on sp^2 hybridized nitrogen orbital) is responsible for the coordination to a variety of metal ions in different oxidation states producing stable metal complexes [3]. Moreover, the presence of electrophilic carbon and nucleophilic nitrogen atoms in the azomethine moiety induces the capability to interact with biological entities such as RNA, DNA, proteins, and lipids [4]. Schiff bases and their metal complexes have not only proved to be useful compounds in medicinal chemistry, but also in other areas of science due to their stability and structural diversity. Indeed, they have found a large number of applications in chemistry, physics, biomedicine, and industry. Some of their specific applications are as followings: i) agents for the qualitative, and quantitative determination of the metal ions [5–7], ii) organic light-emitting diodes (OLEDs) [8,9], iii) electrochemical sensors for determination of anions and cations [5,10], iv) non-linear optical devices [11,12], v) antibacterial, anticancer and antifungal agents in medicinal chemistry [13–18], vi) antitumor agent in clinical as well as experimental tumor chemotherapy [16,19,20], vii) catalyst for ring opening polymerization (ROP), epoxide-ring opening reactions, oxidation, hydroxylation, and hetero-Diels–Alder reactions [21–28],

* Corresponding author.
E-mail address: mghassemzadeh@ccerci.ac.ir (M. Ghassemzadeh).

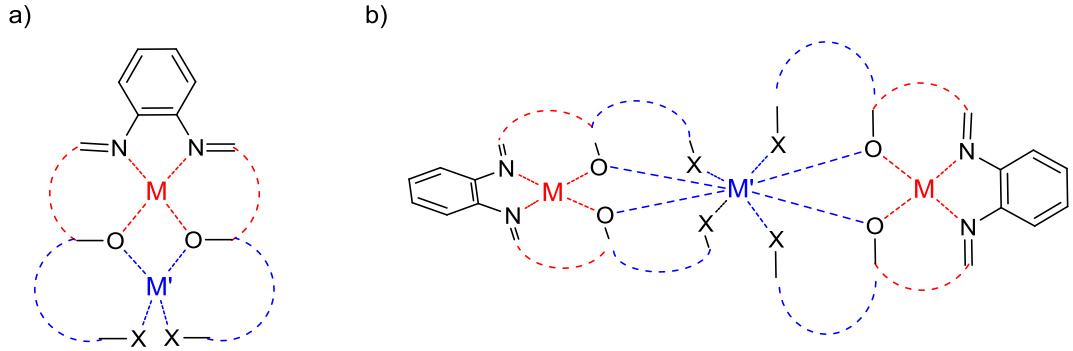

Fig. 1. Representation of a binuclear (a) and trinuclear (b) complex based on a bi-compartmental *bis*-Schiff base ligand showing the locations of its "inner" N_2O_2 (red) and "outer" $O_2X'_2$ (blue) compartments (M and M' are metals having small and large ionic radii, respectively; *X* = donor atom / group containing O, N, S, *etc*. atoms).

viii) building blocks for the preparation of covalent organic frameworks (COF), nanocomposites, and nanoparticles [29–32], ix) corrosion inhibitor for mild steel [33,34], and x) polymeric conductor [35–37].

One of the most important advantages of the Schiff's base reaction is the opening up of the possibility to produce the "multi-azomethine functionalized compounds" from the corresponding multi-carbonyl and/or amine derivatives. Among the "multi-azomethine functionalized compounds", salen and salophen-type *bis*-Schiff bases are extensively studied compounds [38–47]. Over the years, numerous reviews and publications prove the interesting physicochemical properties and potential applications of these compounds and their metal complexes [19,36,43,48-55]. Salen and salophen are prepared by the condensation reaction of one equivalent of 1,2-ethylene/1,2-phenylendiamine with two equivalents of salicylaldehyde derivatives.

From the point view of coordination chemistry, salen and salophen have been recognized as suitable dibasic tetradentate N_2O_2 donor ligands (N_2O_2-compartmental Schiff bases) for the preparation of mononuclear complexes with the transition as well as main group metal ions and are able to stabilize the metal ions in their various oxidation states [53,56-60]. In addition to mononuclear complexes, salens and salophens have also been used to create multinuclear coordination complexes [47,61-66]. Indeed, the nuclearity of the salen and salophen metal complexes can be increased by using macrocyclic- or bi-compartmental N_2O_2-O_2×$_2$ salen and salophen derivatives bearing additional *meta*-positioned donor atoms/groups on their salicylic aromatic ring system (*X* = N, O or S) [59,67-73]. The determined molecular structures of multi-heteronuclear complexes show that the metal ion M (with smaller ionic radius) accommodates in the inner N_2O_2 pocket of the ligand, whereas the other metal ion M' coordinates to the $O_2X'_2$ moiety (Fig. 1).

Amongst bi-compartmental N_2O_2-O_2×$_2$ Schiff bases, those based on *o*-vanilline (3–methoxy salicylaldehyde) are the most studied ones incorporating a $O_2O'_2$ cavity. There are a number of reports dealing with synthesis of complexes based on bi-compartmental N_2O_2-$O_2O'_2$ salen and salophen derivatives involving multi-homonuclear 3d-3d [47,74-78] and 4d-4d metals [79] and multi-heteronuclear 3d-4d [79,80], 3d-4f [36,47,76,81-83], and 4d-4f metals [84,85]. In addition to the afore-mentioned metal combinations, the behavior of some common mononuclear 3d or 4d complexes containing N_2O_2-$O_2O'_2$ bi-compartmental Schiff bases, namely cobalt(II) [77,86], copper(II) [87–89], nickel(II) [87–92], palladium(II) [67] and platinum(II) [93], towards alkali metal ions has already been investigated. These metal combinations have resulted in multi-heteronuclear complexes with diverse molecular structures. Amongst these complexes, the biological activity of few complexes, i.e., copper-sodium and nickel-sodium bearing N,N'-(1,2-phenylene)-bis(3-methoxysalicylideneimine) (H_2L) as Schiff base has been reported [87,91]. Indeed, the presence of *ortho*-positioned methoxy groups on the phenolic ring of the ligand may enhance its cell membrane permeability and its lipophilicity, resulting in better antiproliferative activity [94].

In recent years, sonochemistry has proved to be an efficient, environmentally friendly, simple, time- and energy-saving method for green and sustainable chemical processes. The benefits of this technique in the synthesis of organic or inorganic compounds are shorter reaction times under mild reaction conditions, higher yields, and cost-effectiveness [95]. A literature survey disclosed that this method has already been used for the successful synthesis of numerous applied chemicals and materials, i.e., fabrication of inorganic nanoparticles for applications in catalysis [96], synthesis of organic compounds, pharmaceuticals, and biomaterials [97–101], and preparation of nanostructured materials [102–106]. Indeed, the increasing interest of researchers to use sonochemistry indicates that the sonochemical synthesis is now regarded as a sustainable tool to fabricate applied materials.

During the last decade, novel Pd(II) complexes (as promising metallodrug candidates) have been designed and synthesized. These complexes exhibit greater in vitro as well as in vivo cytotoxicity with respect to a range of cisplatin-resistant cancer cells [107]. They appear to be less toxic and cause lower side effects than conventional anticancer drugs [108,109]. They also display other biological activities such as antiviral, antifungal, antimicrobial, and some of them have already been subjected to clinical trials [110–113].

In our ongoing interest in designing new biologically active Pd(II) complexes (as suitable alternatives to the commonly used Pt(II) complexes) [112,113], we attempted to synthesize two Pd(II)-Na complexes bearing N,N′-(1,2-phenylene)-*bis*(3-methoxysalicylideneimine) ligand. The syntheses of these novel bi-heteronuclear (Pd-Na) and triheteronuclear (Pd-Na-Pd) complexes were successfully achieved *via* a facile, expeditious, and green sonochemical method [95,114]. First, the molecular structure and thermal behavior of both complexes were determined and, subsequently, their in vitro anticancer and antibacterial activities were evaluated. Since sodium is a nontoxic and essential alkali metal ion for human life, it was chosen as the second metal ion in this work.

2. Experimental

2.1. Materials and instruments

The chemicals were purchased from Merck and Fluka and used without further purification. Compound H_2L was prepared according to the literature [115] and was characterized by ^{1}H NMR spec-

troscopy (Fig. SF1). Melting points were recorded on a Büchi B545 melting point apparatus and are uncorrected. Elemental analyses were carried out on a PerkinElmer 2400 CHN Elemental Analyzer. The infrared spectra (Nujol mulls, KBr (4000–400 cm^{-1}), and CsI (500–250 cm^{-1})) were recorded on a Perkin–Elmer 400 spectrometer. ^1H NMR spectra were acquired on a Bruker AQS AVANCE instrument (500 MHz) using Me_4Si ($\delta = 0$ ppm) as internal standard. Thermal gravimetric analyses (TGA) were recorded on a Netzsch TG 209F1 apparatus and on a Mettler-Toledo TGA/SDTA851e thermal analyzer in the temperature range 25–900 °C and 25–800 °C, respectively, with a heating rate of 10 °C/min under air atmosphere. The UV–vis spectra were performed on a Perkin-Elmer Lambda 35 double beam spectrophotometer. The powder X-ray diffraction (PXRD) measurements were carried out using a X'PERT-PRO diffractometer with a Cu anode (λ =1.5406 Å). LC/MS-API analyses were recorded on an Alliance 2695 system. All sonication processes were accomplished using an ultrasonic probe apparatus (Bandelin Sonoplus HD 3100, Bandelin electronic GmbH & Co. KG, Berlin, Germany, microtip MS 72 with a frequency of 20 kHz and amplitude control of 80%).

The microorganisms (*Staphylococcus aureus (ATCC 6538, PTCC 1112)* and *Escherichia coli (ATCC 25,922, PTCC 1399)* used in this study were obtained from the microorganism bank of the Iranian Biological Resource Center. The human breast cancer cell lines, MCF-7, were obtained from the cell bank of Pasteur Institute in Tehran (Iran).

2.2. Synthesis of complexes 1 and 2

Both complexes **1**, i.e. {Na[P*d*L](EtOH)(NO_3)}, and **2**, i.e. {Na[P*d*L]$_2$}Cl, were synthesized under ambient (method A) and ultrasonic (method B) conditions.

Method A: A suspension of H_2L (0.088 g, 0.23 mmol) and palladium(II) acetate (0.051 g, 0.23 mmol) in acetonitrile (10 mL) was stirred thoroughly for two hours at room temperature and then treated with a solution of corresponding sodium salt ($NaNO_3$: 0.02 g, 0.23 mmol or NaCl: 0.006 g, 0.11 mmol) in absolute ethanol (5 mL), and the mixture was stirred for further 24 h at room temperature. The obtained dark orange precipitate was filtered off, washed with cold ethanol (5 mL), dried in air, and used for analyses. **1**: Yield: 0.072 g (60%) and **2**: Yield: 0.14 g (65%).

Method B: An acetonitrile/ethanolic mixture of similar amounts of the reactants as used in method A was sonicated using a microtip sonicator MS 72 at 60 W (80% of maximum power) for 5 and 4 min in order to synthesize complexes **1** and **2**. An orange solid precipitated, which was filtered off and analyzed after similar work-up as described in method A. **1**: Yield: 0.10 g (85%) and **2**: Yield: 0.17 g (80%).

The results of the analyses revealed that the products from both methods A and B were found to be identical.

1: m.p.: > 300 °C (dec.), elemental analysis calculated for $C_{22}H_{18}N_3NaO_7Pd$ (565.80) calcd. C, 46.70; H, 3.21; N, 7.43, found C, 47.00; H, 3.05; N, 7.50%. FT-IR (KBr, cm^{-1}): 2919 (s), 2852 (s), 1606 (s, $\nu_{C=N}$), 1548 (s), 1543 (s), 1464 (s, $\nu_{C=C}$), 1371 (m), 1333 (m), 1243 (s, ν_{C-O}), 1191 (s, ν_{C-O}), 1115 (m), 989 (m), 858 (m), 759 (s), 737 (s), 721 (s), 532 (m). Far-IR (CsI, nujol mulls, cm^{-1}): 532 (w, ν_{Na-O}), 456, 442 (w, $\delta_{O\text{-}Pd\text{-}O}$), 402 (w, ν_{Pd-O}), 300 (w, ν_{Pd-N}); ESI-MS *m/z*: 606 [$M^+ + NH_4^+ + Na^+$], 588 [$M^+ + NH_4^+$], 482 [PdL], 376 [L]; ^1H NMR (500 MHz, DMSO–d_6, ppm) δ 3.78 (s, 6H, OCH_3), 6.61–8.27 (m, 10H, Ar-H), 9.07 (s, 2H, HC=N).

2: m.p.: > 300 °C (dec.), elemental analysis calculated for $C_{44}H_{36}ClN_4NaO_8Pd$ (1020.06) calcd. C, 51.81; H, 3.56; N, 5.49, found C, 50.90; H, 3.42; N, 5.60%. IR (KBr, cm^{-1}): 2919 (s), 2854 (s), 1607 (s, $\nu_{C=N}$), 1519 (m), 1541 (m), 1462 (s, $\nu_{C=C}$), 1377 (s), 128 (m), 1242 (m, ν_{C-O}), 1190 (s, ν_{C-O}), 1109 (m), 982 (m), 856 (w), 735 (m); Far-IR (CsI, nujol mulls, cm^{-1}): 530 (w, ν_{Na-O}), 438 (w, $\delta_{O\text{-}Pd\text{-}O}$), 398 (w, ν_{Pd-O}), 300 (w, ν_{Pd-N}); ESI-MS *m/z*: 1061 [$M^+ + NH_4^+ + Na^+$], 983 [$M^+ + Na^+$], 482 [PdL]; ^1H NMR (500 MHz, DMSO–d_6, ppm) δ 3.79 (s, 12H, OCH_3), 6.62–8.31 (m, 10H, Ar-H), 9.12 (s, 4H, HC=N).

Suitable crystals of **1** and **2** for X-ray diffraction studies were grown by slow evaporation of their filtrates at room temperature after a few weeks.

2.3. Crystal structure analysis of complexes 1 and 2

The selected crystal of **1** and **2** was covered with perfluorinated oil and mounted on a STOE StadiVari single-crystal diffractometer (GaK_α radiation with $\lambda = 1.34143$ Å). The crystallographic data of the complexes are summarized in Table 1. The orientation matrix and the unit cell dimensions were determined from 21484 for **1** and 21449 for **2**. The crystals of **1** and **2** were kept at 180 K during data collection. Using Olex2 [116], the structure was solved with the SHELXT [117] structure solution program using intrinsic phasing and refined with the SHELX [118] refinement package using least squares minimization. All non-hydrogen atoms were refined with anisotropic displacement parameters; hydrogen atoms could be localized and were freely refined.

The crystallographic data have been deposited with the Cambridge Crystallographic Data centre (CCDC) as supplementary publication numbers CCDC-2178864 (**1**) and −2178865 (**2**). Copies of the data can be obtained, free of charge, by application to CCDC, 12 Union Road, Cambridge, CB2 1EZ, UK (fax: +44 1223 336033; Email: data_request@ccdc.cam.ac.uk or *via* the internet: http://www.ccdc.cam.ac.uk/products/csd/request

2.4. In vitro cytotoxic assay

2.4.1. MTT assay

MTT assay was performed on human breast cancer cell lines, MCF-7, for evaluation of cell viability of complexes **1** and **2**. For this purpose, plates of 96 wells were filled with 100 µL culture medium containing 5×10^3 seeded cells and incubated at 37 °C for 24 h. After medium removal, the cells were treated with the above compounds in the range of 0–4 mM. After an incubation time of 24 h, 10 µL of MTT solution (5 mg/mL in RPMI-1640 without phenol red) was added to each well and incubated in darkness at 37 °C for further 4 h to formazan crystal formation. Finally, the media were removed, and the formazan crystals were dissolved by the addition of DMSO (100 µL). The absorbance of the supernatant solution was recorded after 20 min at 570 nm by a Microplate reader (Biotek, BioTec US). Cell viability percentage was determined as follows:

$$\text{cell viability} = (OD_{treated}/OD_{control}) \times 100\%$$

where, $OD_{treated}$ and $OD_{control}$ were the optical density of the treated cells and untreated cells, respectively.

2.5. In vitro antibacterial assay

The antibacterial behavior of complexes **1** and **2** against two bacterial strains was evaluated using the plate colony-counting method. In order to determine the rate of bacterial growth, bacterial suspensions of *S. aureus* (*ATCC 6538, PTCC 1112*) and *E. coli* (*ATCC 25922, PTCC 1399*) were prepared by the direct colony method, where the colonies were taken directly from the plate of fresh-cultivated bacteria and were suspended in sterile 0.9% normal saline. Then, these initial suspensions were adjusted to match the turbidity of a 0.5 McFarland's standard (corresponding to 1.5×10^8 colony forming units (CFU)/mL using 0.05 mL 1.175% w/v $BaCl_2 \cdot 2H_2O$ + 99.5 mL 1% w/v H_2SO_4). The initial suspensions were then 10-fold serially diluted (up to 10^{-2}) in saline (0.9%). The

Table 1
Crystal data and structure refinement for complexes **1** and **2**.

	1	**2**
Emp. Formula	$C_{24}H_{24}N_3NaO_8Pd$	$C_{44}H_{36}ClN_4NaO_8Pd_2$
Formula mass	611.85	1020.01
Crystal size[mm]	0.14 × 0.03 × 0.02	0.05 × 0.04 × 0.01
Crystal system	triclinic	tetragonal
Space group	*P-1*	$I4_1/acd$
a [Å]	8.2248(2)	19.102(1)
b [Å]	11.5511(3)	19.102(1)
c [Å]	14.5302(4)	51.582(5)
α [°]	112.713(2)	90
β [°]	96.424(2)	90
γ [°]	90.301(2)	90
Volume [Å3]	1263.63(6)	18821(3)
Z	2	16
$D_{calcd.}$ [g·cm^{-3}]	1.608	1.440
Absorp. Correct.	multi-scan	multi-scan
μ [cm^{-1}]	4.362	4.800
F(000)	620.0	8192.0
Temp.[K]	180	180
2Θ range for data collection/ °	5.78 to 124.994	6.426 to 100
Index range		
h	−10→10	−21→20
k	−5→15	−31→21
l	−19→17	−58→58
Reflect. Collected	15830	73747
Radiation	Ga K_α ($\lambda = 1.34143$)	Ga K_α ($\lambda = 1.34143$)
Independent Reflect. (R_{int}, R_{sigma})	5950 (0.0211, 0.0282)	3676 (0.1664, 0.0732)
Reflect. with I ≥ 2σ (I)	5068	2168
Parameters	338	277
Goodness-of-fit on F^2	1.011	0.849
Final R indexes [I ≥ 2σ (I)]	$R_1 = 0.0310$, $wR_2 = 0.0800$	$R_1 = 0.0383$, $wR_2 = 0.0878$
Final R indexes [all data]	$R_1 = 0.0369$, $wR_2 = 0.0813$[a]	$R_1 = 0.0690$, $wR_2 = 0.0919$[b]
Largest diff. peak/hole / e Å^{-3}	0.45/−1.23	0.62/−0.28
CCDC number	2178864	2178865

[a] $w = 1/[\sigma^2(F_o^2) + (0.0567 \cdot P)^2]$; $P = [\max(F_o^2, 0) + 2 \cdot F_c^2]/3$ and [b] $w = 1/[\sigma^2(F_o^2) + (0.1281\ P)^2]$; $P = [\max(F_o^2, 0) + 2 \cdot F_c^2]/3$.

concentration of the resulting suspension was 1.5×10^6 CFU/mL, which was also used as the control sample (blank samples). On the other hand, the solutions of the complexes in dimethyl sulfoxide (5 mM) were prepared by dissolving 10 mmol each of the substances (**1**: 5.65 mg and **2**: 10.20 mg) in DMSO (2 mL) and used as test substances. The bacterial suspensions (2 mL) were next spread over the surface of nutrient agar plates containing the test substances (0.5 mL). The plates were allowed at ambient temperature for 24 h and incubated for 24 h at 37 °C. The samples were 10-fold serially diluted in saline (up to 10^{-5}), and 1 mL of each dilution was transferred to agar plates. The number of survived bacterial colonies (measured in CFUs) was quantitated after cultivation at ambient temperature for 24 h and subsequent incubation of the plates at 37 °C for 24 h. The rates of colony-forming units (R) were calculated considering the dilution factor by the following equation:

$$R = [(N\,\text{control} - -N\,\text{sample})/N\,\text{control}] \times 100\,\%$$

where, N control and N sample are the average numbers of the bacterial colony of the control sample (containing no antibacterial agent) and complex test samples, respectively. All tests were performed in triplicate.

3. Results and discussion

3.1. Synthesis and characterization

The treatment of a mixture of H_2L and palladium(II) acetate with $NaNO_3$ in a molar ratio of 1:1:1 and NaCl in a molar ratio of 2:2:1 in ethanol leads to the formation of binuclear complex{Na[P*d*L](EtOH)(NO_3)} (**1**) and trinuclear complex {Na[P*d*L]$_2$}Cl (**2**), respectively, at room temperature and under ultrasonic condition (Scheme 1). Amongst the employed methods, ultrasonics proved to be the most effective one resulting in high to excellent yields (**1** = 85%, and **2** = 80%). The orange-colored complexes **1** and **2** are found to be air-stable solids.

In ^{1}H NMR spectra of H_2L recorded in DMSO–d_6 at room temperature (Fig. SF1), the peaks of the benzene rings are observed at $\delta = 6.90$ – 7.46 ppm having an integral of 10H. Furthermore, the observed peaks at $\delta = 3.82$, 8.93, and 13.01 ppm can be attributed to the protons of *meta*-positioned methoxy groups, protons of the azomethine moieties, and *ortho*-positioned hydroxyl groups, respectively (assigned protons a and c in Scheme 1). The peaks of the *ortho*-positioned hydroxyl groups were not observed in the ^{1}H NMR spectra of complexes **1** and **2** indicating the twofold deprotonation of the ligand upon coordination to the palladium ion (Figs. SF2 (**1**) and SF3 (**2**)). In ^{1}H NMR spectra of complexes **1** and **2**, the peak of protons of azomethine groups were observed at $\delta = 9.07$ ppm (**2**), and 9.12 ppm (**3**), and the corresponding peaks of the benzene rings were observed at $\delta = 6.60$ – 8.27 ppm (**1**) and 6.60 – 8.31 ppm (**2**). Interestingly, the peak of the protons of azomethine groups and the peak of one proton of the salophen ring of both complexes (assigned protons a and b, respectively, Scheme 1) underwent a downfield shift with respect to the free ligand as a consequence of the coordination to the metal center. This phenomenon has also been observed in UV spectra of the ligand and both complexes (Fig. 2). The UV spectra of the ligand show two electronic transitions (ETs) at 291 nm and 341 nm, which may

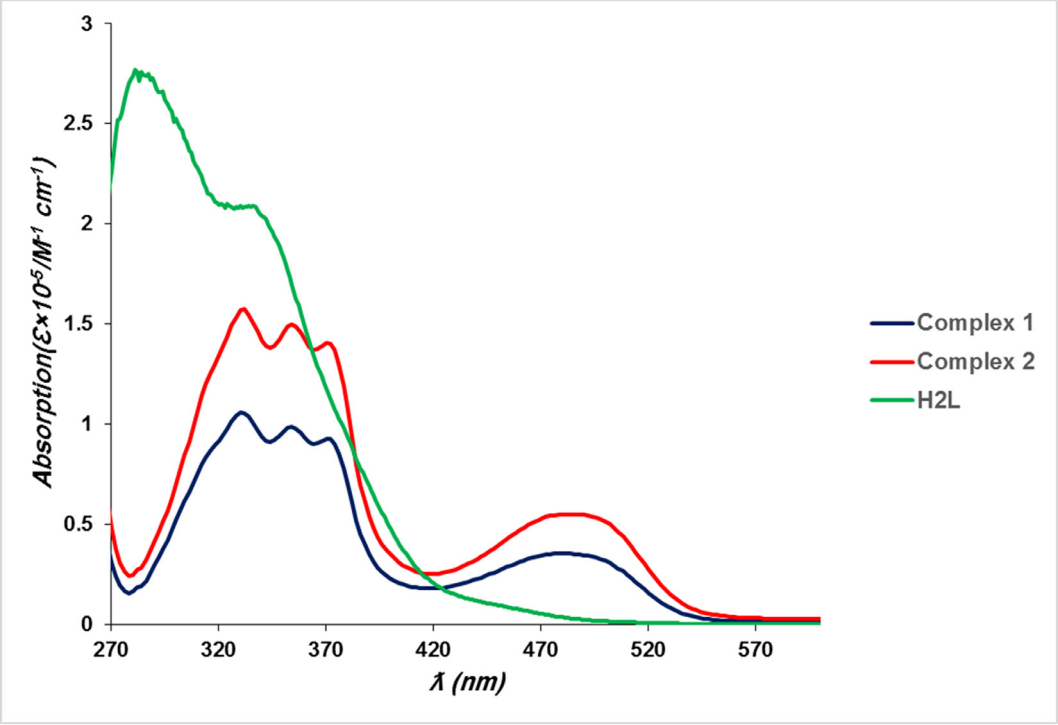

Fig. 2. UV–visible spectra of ligand H_2L and complexes **1** and **2**.

be assigned to the intra-ligand charge transfers ($\pi \rightarrow \pi^*$ or $n \rightarrow \pi^*$ transitions). In UV spectra of both complexes, the intra-ligand transitions observed at 334 nm and 358 nm show redshift and lower intensities with respect to the free ligand. Furthermore, the appearance of an additional new ET at 374 nm in the UV spectra of complexes **1** and **2** indicates another arrangement of π-electrons (π-electronic conjugation) in the twofold deprotonated ligand in both of them relative to the free ligand. The latter can be assigned to the ligand-to-metal charge transfer (LMCT). Moreover, the presence of a further new transition at 490 nm in the UV spectra of both complexes, which can be assigned to the metal-to-ligand charge transfer (MLCT), confirms the formation of the complexes.

In FT-IR spectra of multinuclear complexes, the absorption bands due to aromatic C=C, C=N, C–$O_{phenolic}$ and C–$O_{methoxy}$ stretching modes were observed at 1464, 1606, 1243, and 1191 cm^{-1} for **1**, and 1462, 1607, 1242, and 1190 cm^{-1} for **2** (Figs. SF4 and SF5). The shift of C=N, C–$O_{phenolic}$, and C–$O_{methoxy}$ stretching vibrations of the free ligand (1608, 1251, and 1203 cm^{-1}, respectively) to lower wavenumbers indicates the coordination of ligand to metal center through these moieties. Similar C=N, C–$O_{phenolic}$, and C–$O_{methoxy}$ stretching vibrations were also reported for palladium(II) complex based on *o*-vanilline Schiff base (1603, 1245, and 1201, respectively) [119].

Additionally, in complexes **1** and **2**, azomethine, phenolic, and methoxy moieties are involved in the coordination with metal centers. Indeed, upon complexation, new vibration bands appear in the Far-IR spectra of **1** (at 532, 402, 300, and 442 cm^{-1}) and **2** (at 530, 398, 300, and 438 cm^{-1}), which can be attributed to the Na-O, Pd-O, Pd-N stretching vibrations and O-Pd-O deformation vibrations, respectively (Figs. SF6 and SF7) [112,120,121]. Electrospray-ionization mass spectra (ESI-MS) of complexes **1** and **2** registered in methanol show the mass peaks at $m/z = 606$ and 1061, respectively, corresponding to their $[M^+ + Na^+ + NH_4^+]$ fragments. In addition, other fragments corresponding to the principal scissions of each complex are assigned in Figs. SF8 (**1**) and SF9 (**2**).

3.2. Crystal structure description of complexes 1 and 2

Selected bond lengths and bond angles of complexes **1** and **2** are listed in Table ST1.

The yellowish single crystals of **1** (needles) and **2** (plates) were grown from their mother liquids using slow evaporation method.

The molecular structure determination of complexes **1** and **2** revealed that the former crystallizes in the triclinic space group *P-1* with two {Na[Pd*L*](NO_3)(EtOH)} molecules, whereas the latter crystallizes in tetragonal space group $I4_1/acd$ containing 16 {Na[Pd*L*]$_2$}Cl molecules per unit cell. Both complexes are based on [PdL]-units. The molecular structure of the neutral complex **1** can be described as an adduct of this unit with [Na(NO_3)(EtOH)] moiety (Fig. 3), whereas that of the ionic complex **2** consists of two over one sodium ion connected [PdL] units as cation and one chlorine anion (Fig. 4).

According to the determined molecular structures of both complexes, Pd(II) ion in the [PdL] unit, showing essentially identical metal coordination environment, is located in the N_2O_2-inner sphere of the twofold deprotonated Schiff base (L). It is coordinated to two iminic nitrogen atoms and two phenolate oxygen atoms in a very slightly distorted square planar geometry (the O-Pd-N *trans* angles are found to be 178.95(5) ° and 179.68(3) ° for **1** and 177.4(2) and 179.6(2) ° for **2**). The mean Pd-N and Pd-O bond lengths are 1.948 and 1.972 Å for **1** and 1.935 and 1.967 Å for **2**, respectively. They are similar to those found in other structurally characterized palladium(II) salophen-type complexes [119,122].

In neutral complex **1**, the sodium atom is hosted in the outer $O_2O'_2$ compartment of the twofold deprotonated Schiff base (L) interacting with its all four oxygen atoms (Na-O bond distances of mean 2.379 Å and Na-O' bond lengths of mean 2.664 Å). The observed Na-O bond distances are analogous to those reported by Cunningham and coworkers [123] for [Na(NO_3)MeOH]·NiL4 (**3**, mean Na-O: 2.358 Å) and [Na(NO_3)MeOH]·CuL1 (**4**, mean Na-O: 2.347 Å) containing similar salen type Schiff base ligands. These bond lengths are significantly shorter than those found

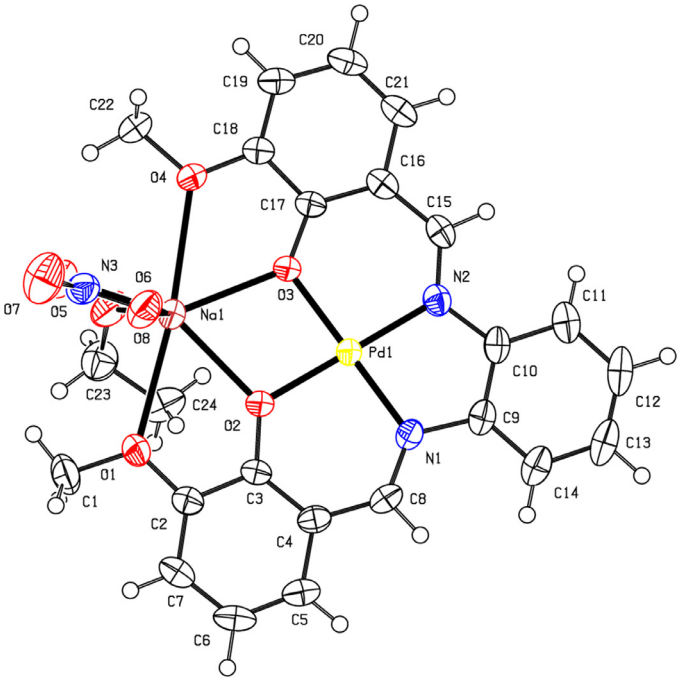

Fig. 3. Representation of molecular structure of complex **1** (thermal ellipsoids are depicted at the 50% probability level).

by Asakawa and coworkers [67] for Pd-Na-binuclear complexes $[Pd_2Na_2L1_2(\mu\text{-}OH_2)_2](ClO_4)_2(CH_2Cl_2)_3$ (**5**, mean Na-O: 2.594 Å) and $[Pd_2Na_2(L1)_2]$-$(CH_3CN)_2(C_3H_6O)_2$ (**6**, mean Na-O: 2.974 Å) incorporating a salophen crown ether macrocyclic ligand H_2L1. The Na-O' bond lengths in **1** (mean 2.664 Å) are longer than those of complexes **3** (mean Na-O': 238.2 Å) and **4** (mean Na-O': 2.593 Å) but shorter than those of **5** (mean Na-O': 2.758 Å). The sodium atom is further involved in interactions with two oxygen atoms of the nitrate moiety (Na1-O5: 2.487(2) Å and Na1-O6: 2.489(2) Å) and an ethanol oxygen atom, *trans* to the nitrate moiety (Na1-O8: 2.331(2) Å). These arrangements result in seven-coordination geometry about the sodium.

In the trinuclear $\{[PdL]_2Na\}^+$- cation of **2**, the sodium ion is coordinated to two phenolate and two methoxy oxygen atoms of each [PdL] unit exhibiting similar mean Na-O and Na-O' bond lengths (2.391 Å and 2.677 Å, respectively) as observed in complex **1**. Therefore, the Na^+ ion is eight-coordinated in a trigonal-dodecahedron geometry and is in an approximately linear arrangement with the two palladium(II) centers (Pd-Na-Pd: 172.94(8)°). Similar arrangements of sodium and 3d metal ion have been observed in the Ni_2Na-trinuclear-Schiff base complex [Ni(vanen)Na(vanen)Ni]BF_4] and [(NiL')Na(NiL')]ClO_4, where [H_2vanen = N,N'-ethylene-*bis*(3-methoxysalicylideneimine) and H_2L' = N,N′-(1,2-phenylene)-*bis*(3-methoxysalicylidene-imine), respectively] [124,125]. Furthermore, the chloride anion in this complex is disordered over two positions with an occupancy factor of 0.5.

In complex **2**, the observed dihedral angle between the "best planes" through NaOPdO units is 80.00(5)° indicating the orthogonal orientation of the [PdL] moieties in the complex.

In both complexes **1** and **2**, the Pd···Na intermetallic distances are 3.451(1) Å (Pd1···Na1) and 3.439(1) Å (Pd1···Na1 and Pd1'···Na1), respectively, which are slightly shorter than the sum of van der Waals radii of "Pd···Na" (3.90 Å) [126]. They are significantly shorter than the Pd···Na distances reported for Pd-Na-multinuclear complexes **5** (Pd···Na: 3.599(3) Å) and 3.669(3) Å) and **6** (Pd···Na (3.939(2) Å) [67].

3.3. Thermal gravimetric analysis

The thermal property of complexes **1** and **2** was studied using the thermal gravimetric analysis technique (TGA). The investigations were carried out in the temperature range of 25 °C to 900

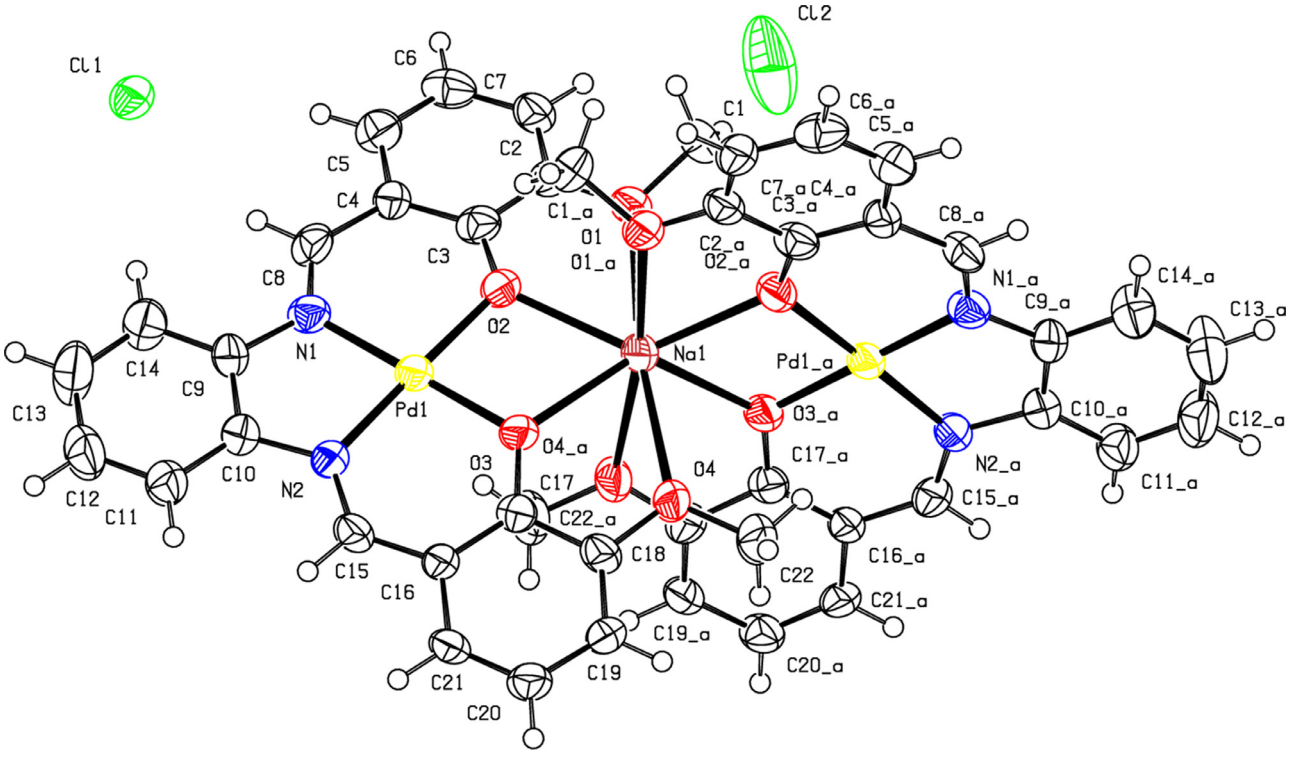

Fig. 4. Representation of molecular structure of complex **2** (thermal ellipsoids are depicted at the 50% probability level).

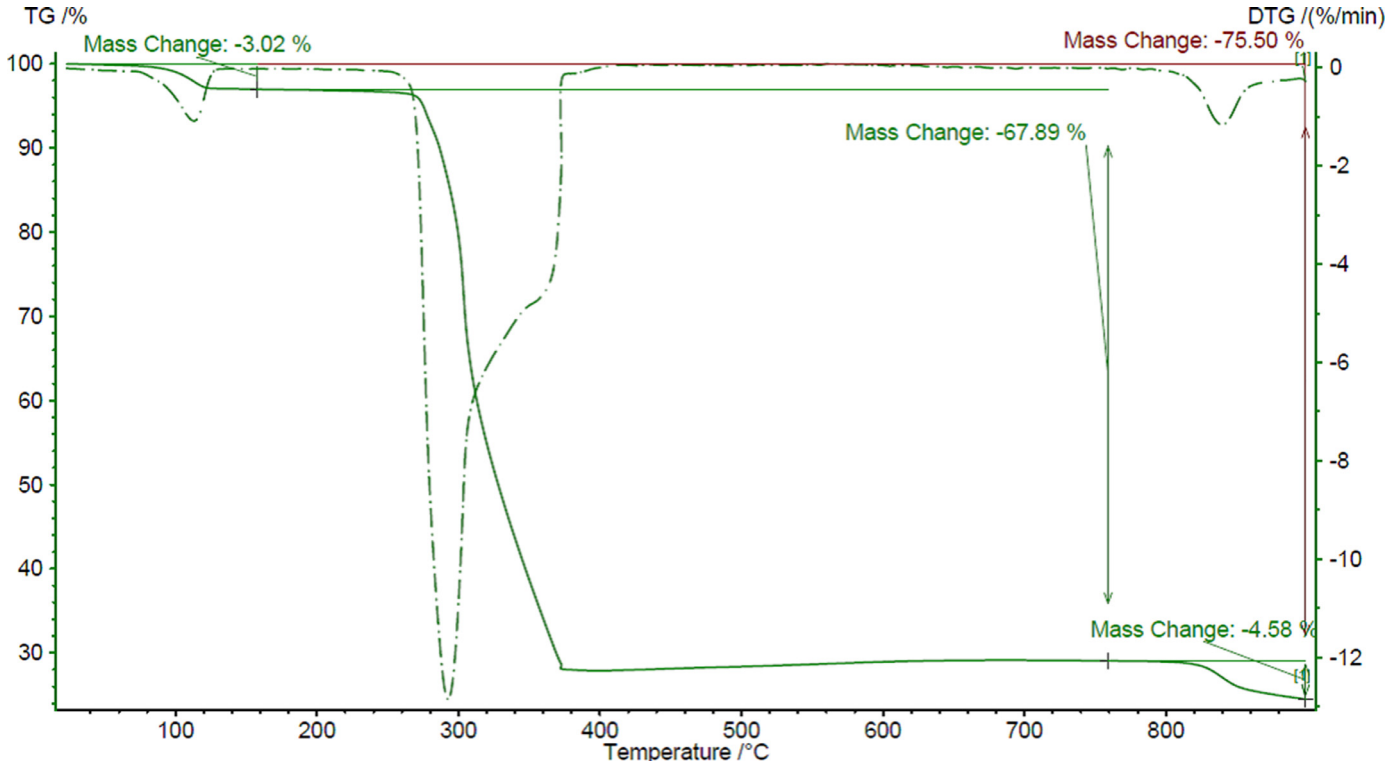

Fig. 5. TGA curve of complex **1**.

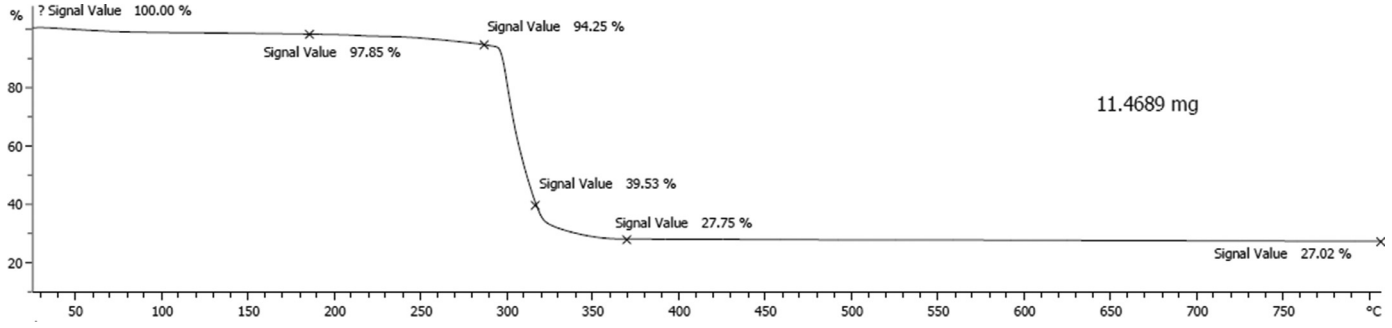

Fig. 6. TGA curve of complex **2**.

°C for complex **1** (Fig. 5) and from ambient temperature to 800 °C for complex **2** (Fig. 6) with a heating rate of about 10 °C/min in an air atmosphere.

The TG curve of complex **1** undergoes a decomposition process over three stages. The initial weight loss from ambient temperature to 110 °C is associated with the removal of ethanol molecule (found: 3.50%; calcd.: 3.02%). The observed weight loss in the temperature region of 260 – 450 °C is related to the decomposition of ligand along with one nitric oxide (*L*+NO; found: 68.94%, calcd.: 67.89%). The TG analysis of complex **1** revealed that the final product of the thermal decomposition of the complex at 900 °C is a composition of 2Pd+Na+2O (found: 24.74%, calcd.: 24.50%).

The TGA spectra of {[P*d*L]$_2$Na}Cl (**2**) demonstrate the removal of an ethanol molecule below 280 °C (found: 3.6%, calcd.:3.1%) followed by the loss of the ligand in the range of 300–360 °C (found: 73.33%, calcd.: 72.25%). The TG analysis of complex **2** displays that the final product of its thermal decomposition at 800 °C consists of a composition of two palladium, one sodium, one chlorine atom, and one oxygen atom (2Pd+Na+Cl+O; found: 27.02%, calc: 26.51%).

In order to find out the chemical composition of compounds occurring after the decomposition of the ligand, pyrolysis of the complexes was carried out at 500 °C. The chemical composition of the post-pyrolysis samples **P1**, and **P2** was determined by energy-dispersive X-ray spectroscopy (EDX) and X-ray powder diffraction (XRD).

EDX analyses of **P1**, and **P2** (Figs. SF10 and SF11, respectively) show the presence of the palladium, sodium and oxygen elements in sample **P1** and palladium, sodium, oxygen, and chlorine elements in sample **P2**.

The X-ray diffractogram of the samples **P1** and **P2** were recorded in the range of $2\theta = 25 - 70°$. XRD pattern indicates that all samples have well-defined crystalline structures. Furthermore, the broadening of their peaks pointed out the generation of nanoscaled structures. The mean crystallite size of the components of each sample can be determined from Scherrer's formula [127],

$$D = \frac{0.9\lambda}{B(\theta)cos(\theta)}$$

where D is the crystallite diameter, λ the wavelength, θ the Bragg angle, and $B(\theta)$ the full width at half maximum (FWHM) of the major peak of each compound. The position and FWHM values of the major peak of each component in samples **P1** and **P2**, and their mean crystallite size are summarized in Table 2.

Table 2
The position of the major peak, its FWHM and calculated mean crystallite size of the nanoscaled samples **P1 and P2**.

Sample	Peak position, 2θ (°)	FWHM	mean crystallite size (nm)
P1			
Pd	40.24	0.17	49
PdO	34.02	0.20	42
NaO_2	32.42	0.10	84
P2			
Pd	40.18	0.17	49
PdO	33.97	0.20	42
NaCl	31.78	0.12	67

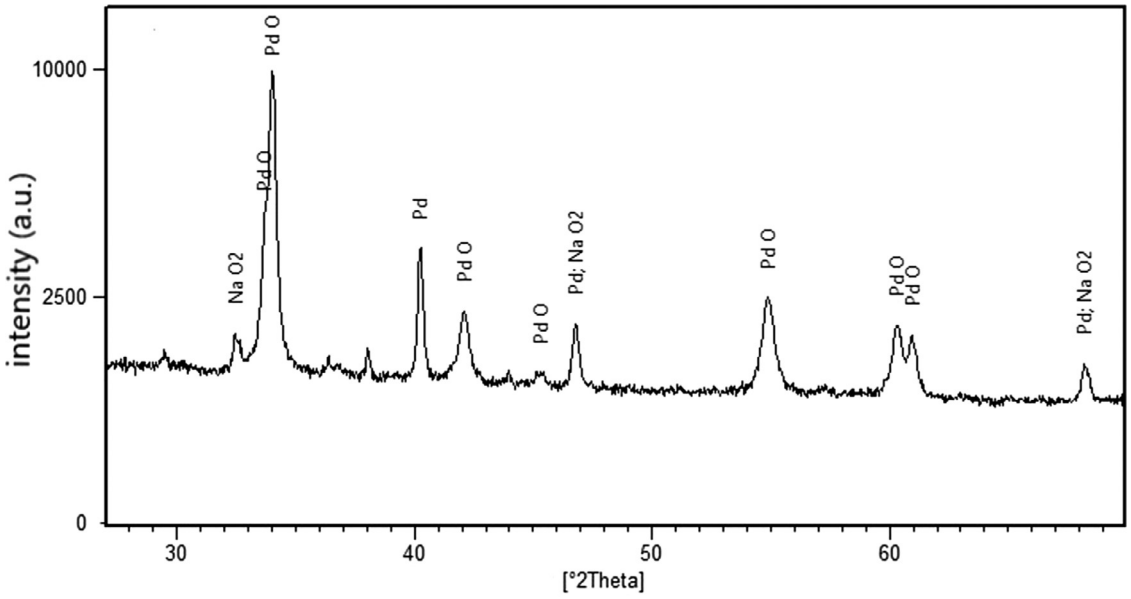

Fig. 7. Powder XRD pattern of sample **P1** obtained from the solventless thermolysis of complex **1** at 500 °C in air.

In the XRD pattern of sample **P1** (Fig. 7), three phases could be identified. The observed reflection planes (111), (200), (220), (311) and (222) correspond to a Pd(0) phase (JCPDS-No.: 01–087–0639: cubic structure of Pd with lattice constants $a=b=c=5.327$ Å, $\alpha=\beta=\gamma=90.0°$, and the Fm-3 m symmetry space group). Also, the reflection planes (022), (101), (110), (111), (112), (103), (200), (004) (202) and (211) could be attributed to PdO phase (JCPDS-No.: 01–075–0584: tetragonal structure of PdO with lattice constants $a=b=3.036$ and $c=3.88$ Å, $\alpha=\beta=\gamma=90.0°$, and the P-4n2 symmetry space group). The third one has been identified as the NaO_2 phase showing the reflection planes of (111), (200), (220), (311), (222), (400), (331), (420), and (422). The latter planes are in agreement with JCPDS-No.: 01–077–0207 (cubic structure of NaO_2 with lattice constants $a=b=c=5.512$ Å, $\alpha=\beta=\gamma=90.0°$ and the Fm-3 m symmetry space group). The mean crystallite size determined from the Debye–Scherrer equation for the Pd, PdO, and NaO_2 phases were found to be 49 nm, 42 nm, and 84 nm, respectively.

The X-ray diffractogram of sample **P2** represents also a combination of the characteristic peaks of three compounds (Fig. 8), namely Pd, PdO and NaCl, i.e. reflection planes of (111), (200), (220), (311), (222), (400), (331) and (420) for Pd (JCPDS-No.00–046–1043, cubic structure of Pd with lattice constants $a=b=c=3.89$ Å, $\alpha=\beta=\gamma=90.0°$, and the Fm3m symmetry space group), reflection planes of (022), (101), (110), (111), (112), (103), (200), (004), (202) and (211) for PdO (JCPDS-No.: 01–075–0584), and those at (200), (220), (311), (222), (400), (331), (420), (422) and (640) for NaCl (JCPDS-No.: 00–001–0994, cubic structure of NaCl with lattice constants $a=b=c=5.628$ Å, $\alpha=\beta=\gamma=90.0°$, and the Fm3m symmetry space group). The Debye–Scherrer calculations indicate that the mean crystallite size for the Pd, PdO, and NaCl phases in complex **3** is 49 nm, 42 nm, and 67 nm, respectively.

3.4. In vitro cytotoxic activity

The cytotoxicity of complexes **1** and **2** towards the breast cancer cell line (MCF-7) was evaluated using an MTT toxicity assay. The results revealed that the cell viability decreased with the increase of concentration from 0 to 1 mM to point out that the treatment was dose-dependent. Moreover, the cytotoxic concentration values of the tested compounds for the death of 50% of viable cells (CC50) were found to be 103 μM and 89 μM for **1** and **2**, respectively, evidencing the higher cytotoxicity effect of complex **2** compared to complex **1**. Fig. 9 demonstrates the anticancer activity of two palladium(II) complexes towards MCF-7 breast cancer cells. It is noteworthy to mention that both compounds displayed notable cytotoxicity, whereas carboplatin (as a standard anticancer drug) exhibited no anticancer effect towards this cell line at the same concentration range within 24 h of incubation.

3.5. In vitro antibacterial activity

The in vitro antibacterial activity of both palladium(II) complexes was investigated against two pathogenic bacterial strains, one gram-negative (*E. coli* ATCC 25922, PTCC 1399) and one gram-positive bacterial strain (*S. aureus* ATCC 6538, PTCC 1112). The results of the antibacterial investigations are summarized in Table 3. According to the results, both complexes show high antibacterial activity towards gram-negative bacterial strains, i.e., 85.00% for **1**

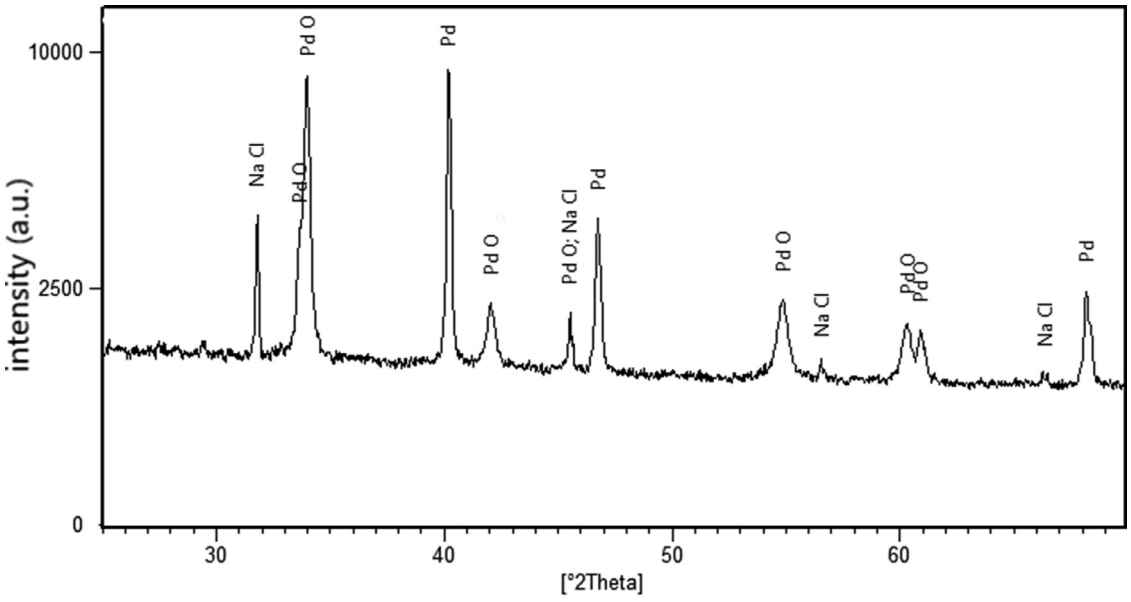

Fig. 8. Powder XRD pattern of sample **P2** obtained from the solventless thermolysis of complex **2** at 500 °C in air.

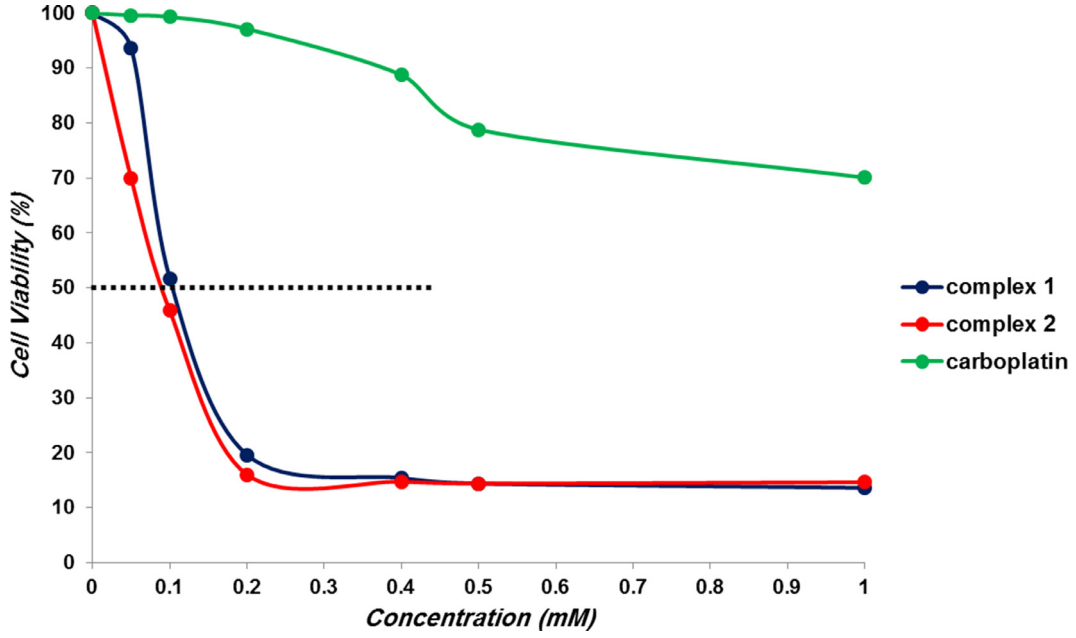

Fig. 9. The cell viability percentage of MCF-7 against various concentrations of binuclear complex **1** and trinuclear complex **2** after 24 h using MTT assay.

and 88.00% for **2**. On the other hand, the same compounds exhibit a lesser effect on gram-positive bacterial strains resulting in moderate activity, i.e. 60.00% for **1** and 66.00% for **2**. Furthermore, as depicted in Table 3, **1** exhibited lower antibacterial activity towards both bacterial strains than complex **2**.

4. Conclusions

This report deals with the rapid sonochemical preparation of two novel bi- and trinuclear palladium(II)–sodium complexes incorporating an *o*-vanilline bicompartmental Schiff base. In both complexes, each Pd(II) ion is located in the N_2O_2 inner sphere of the twofold deprotonated Schiff base in a *cis* arrangement, whereas the sodium ion is placed in the $O_2O'_2$ outer sphere of the Schiff base. The sodium atom in binuclear complex **1** is hepta coordinated, whereas it adopts a trigonal dodecahedral coordination geometry in the trinuclear complex **2**.

In addition, the solventless thermolysis of both complexes at 500 °C was also studied by thermal gravimetric analysis (TGA). EDX and powder XRD data pointed out the presence of highly pure nanoscaled materials, i.e., an ensemble of Pd, PdO, and NaO_2 for **1** (mean crystallite size: 49, 42 and 84 nm, respectively) and an ensemble of Pd, PdO, and NaCl for **2** (mean crystallite size: 49, 42 and 67 nm, respectively).

Subsequently, the in vitro cytotoxicity of bi- and trinuclear complexes **1** and **2** were investigated against human breast cancer cell lines (MCF-7) showing IC50 values of 103 µM for **1** and 89 µM for **2**. This is while carboplatin (a standard anticancer drug) exhibited no cytotoxicity at the same concentration. Furthermore, both complexes exhibited moderate to high antibacterial activity against two bacterial pathogens (*S. aureus* and *E. coli*).

Table 3
Colony numbers and the antibacterial rates for complexes **1** and **2**, and control samples against *E. coli* and *S. aureus* bacterial strains.

Microorganism	Sample	CFU/mL	Antibacterial rates (%)
E. coli	**1**	2.2×10^5	85.00
(***ATCC 25922***)	**2**	1.8×10^5	88.00
	Control	1.5×10^6	–
S. aureus	**1**	6.0×10^5	60.00
(***ATCC 6538***)	**2**	5.1×10^5	66.00
	Control	1.5×10^6	–

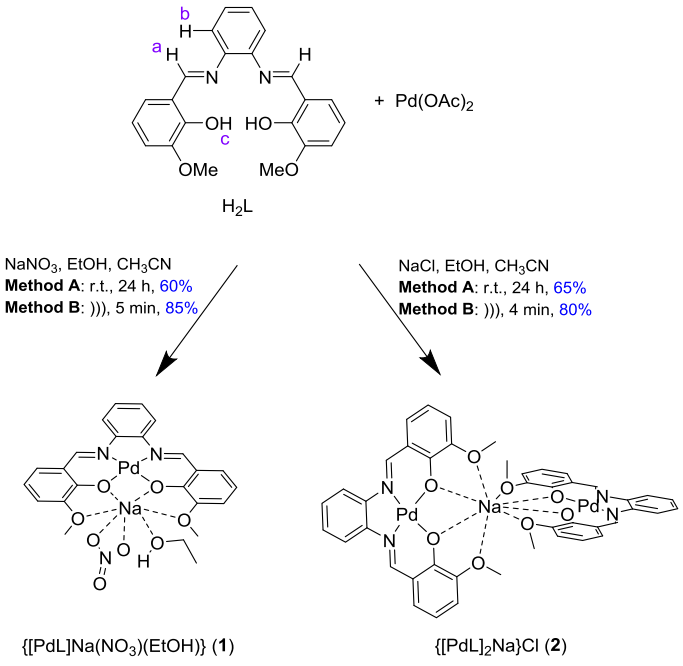

Scheme 1. Synthesis routes for the preparation of complexes **1** and **2**.

Electronic Supplementary Information (ESI)

The Supporting Information is available on the Elsevier Publications Website at DOI: ****.

- ^{1}H NMR spectra of H_2L and complexes **1** and **2** (Figs. SF1 – SF3).
- FT- and Far-IR spectra of complexes **1** and **2** (Figs. SF4 – SF7).
- ESI-MS spectra of complexes **1** and **2** (Figs. SF8 and SF9).
- EDX analysis of the samples **P1** and **P2** (Figs. SF10 – SF11).
- Selected bond lengths and bond angles of complexes **1** and **2** (Table ST1).

Declaration of Competing Interest

The authors declare that they have no known competing financial interests or personal relationships that could have appeared to influence the work reported in this paper.

CRediT authorship contribution statement

Atousa Goudarzi: Investigation, Methodology. **Maryam Saeidifar:** Investigation, Writing – original draft, Writing – review & editing. **Kioumars Aghapoor:** Formal analysis, Writing – review & editing. **Farshid Mohsenzadeh:** Writing – review & editing. **Dieter Fenske:** Formal analysis, Writing – review & editing. **Olaf Fuhr:** Formal analysis, Writing – review & editing. **Mitra Ghassemzadeh:** Project administration, Conceptualization, Writing – original draft, Writing – review & editing.

Data Availability

Data will be made available on request.

Supplementary materials

Supplementary material associated with this article can be found, in the online version, at doi:10.1016/j.molstruc.2022.134224.

References

[1] H. Schiff, Mitteilungen aus dem Universytaetslaboratorium in Pisa: eine neue Reihe organischer Basen, Justus Liebigs Ann. Chem. 131 (1864) 118–119 doi-jlac.18641310113.
[2] T.T. Tidwell, Hugo (Ugo) Schiff, Schiff bases, and a century of b-lactam synthesis, Angew. Chem. Int. Ed. 47 (2008) 1016–1020, doi:10.1002/anie.200702965.
[3] A. Hameed, M. Al-Rashida, M. Uroos, S. Abid Ali, K.M. Khan, Schiff bases in medicinal chemistry: a patent review (2010–2015), Expert Opin. Ther. Pat. 27 (2017) 63–79, doi:10.1080/13543776.2017.1252752.
[4] Z.H. Chohan, M. Arif, Z. Shafiq, M. Yaqub, C.T. Supuran, In vitro antibacterial, antifungal & cytotoxic activity of some isonicotinoylhydrazide Schiff's bases and their cobalt (II), copper (II), nickel (II) and zinc (II) complexes, J. Enzyme Inhib. Med. Chem. 21 (2006) 95–103, doi:10.1080/14756360500456806.
[5] A.L. Berhanu, I. Mohiuddin Gaurav, A.K. Malik, J.S. Aulakh, V. Kumar, K.-.H. Kim, A review of the applications of Schiff bases as optical chemical sensors, TrAC Trends Anal. Chem. 116 (2019) 74–91, doi:10.1016/j.trac.2019.04.025.
[6] W. Ding, Y. Wu, Sustainable dialdehyde polysaccharides as versatile building blocks for fabricating functional materials: an overview, Carbohydr. Polym. 248 (2020) 116801, doi:10.1016/j.carbpol.2020.116801.
[7] M. Kaur, S. Kumar, M. Yusuf, J. Lee, R.J. Brown, K.H. Kim, A.K. Malik, Post-synthetic modification of luminescent metal-organic frameworks using Schiff base complexes for biological and chemical sensing, Coord. Chem. Rev. 449 (2021) 214214, doi:10.1016/j.ccr.2021.214214.
[8] J. Zhang, L. Xu, W.-.Y. Wong, Energy materials based on metal Schiff base complexes, Coord. Chem. Rev. 35 (2018) 180–198, doi:10.1016/j.ccr.2017.08.007.
[9] C.C. Vidyasagar, B.M. Muñoz Flores, V.M. Jimenez-Perez, P.M. Gurubasavaraj, Recent advances in boron-based Schiff base derivatives for organic light-emitting diodes, Mater. Today Chem. 11 (2019) 133–155, doi:10.1016/j.mtchem.2018.09.010.
[10] M.K. Goshisht, G.K. Patra, N. Tripathi, Fluorescent Schiff base sensors as a versatile tool for metal ion detection: strategies, mechanistic insights, and applications, Mater. Adv. 3 (2022) 2612–2669, doi:10.1039/D1MA01175H.
[11] S. Celedón, V. Dorcet, T. Roisnel, A. Singh, I. Ledoux-Rak, J.R. Hamon, D. Carrillo, C. Manzur, Main-chain oligomers from Ni^{II}- and Cu^{II}-centered unsymmetrical N_2O_2 Schiff-base complexes: synthesis and spectral, structural, and second-order nonlinear optical properties, Eur. J. Inorg. Chem. 4 (2014) 4984–4993, doi:10.1002/ejic.201402469.
[12] M.S. More, S.B. Pawal, S.R. Lolage, S.S. Chavan, Syntheses, structural characterization, luminescence and optical studies of Ni(II) and Zn(II) complexes containing salophen ligand, J. Mol. Struct. 1128 (2017) 419–427, doi:10.1016/j.molstruc. 2016.08.083.
[13] C.M. Da Silva, D.L. da Silva, L.V. Modolo, R.B. Alves, M.A. de Resende, C.V.B. Martins, Â.de Fátima, Schiff bases: a short review of their antimicrobial activities, J. Adv. Res. 2 (2011) 1–8, doi:10.1016/j.jare.2010.05.004.
[14] A. Kajal, S. Bala, S. Kamboj, N. Sharma, V. Saini, Schiff bases: a versatile pharmacophore, J. Catal. (2013) 1–14, doi:10.1155/2013/893512.
[15] M.S. More, P.G. Joshi, Y.K. Mishra, P.K. Khanna, Metal complexes driven from Schiff bases and semicarbazones for biomedical and allied applications: a review, Mater. Today Chem. 14 (2019) 100195, doi:10.1016/j.mtchem.2019.100195.
[16] P. Ghanghas, A. Choudhary, D. Kumar, K. Poonia, Coordination metal complexes with Schiff bases: useful pharmacophores with comprehensive biological applications, Inorg. Chem. Commun. 130 (2021) 108710, doi:10.1016/j.inoche.2021.108710.
[17] M. Pervaiz, S. Sadiq, A. Sadiq, U. Younas, A. Ashraf, Z. Saeed, M. Zuber, M. Adnan, Azo-Schiff base derivatives of transition metal complexes as antimi-

crobial agents, Coord. Chem. Rev. 447 (2021) 214128, doi:10.1016/j.ccr.2021.214128.
[18] J. Ceramella, D. Iacopetta, A. Catalano, F. Cirillo, R. Lappano, M.S. Sinicropi, A review on the antimicrobial activity of Schiff bases: data collection and recent studies, Antibiotics 11 (2022) 191, doi:10.3390/antibiotics11020191.
[19] M.A. Malik, O.A. Dar, P. Gull, M.Y. Wani, A.A. Hashmi, Heterocyclic Schiff base transition metal complexes in antimicrobial and anticancer chemotherapy, Med. Chem. Commun. 9 (2018) 409–436, doi:10.1039/c7md00526a.
[20] D. Iacopetta, R. Lappano, A. Mariconda, J. Ceramella, M.S. Sinicropi, C. Saturnino, M. Talia, F. Cirillo, F. Martinelli, F. Puoci, C. Rosano, P. Longo, M. Maggiolini, Newly synthesized imino-derivatives analogues of resveratrol exert inhibitory effects in breast tumor cells, Int. J. Mol. Sci. 21 (2020) 7797, doi:10.3390/ijms 21207797.
[21] E.N. Jacobsen, F. Kakiuchi, R.G. Konsler, J.F. Larrow, M. Tokunaga, Enantioselective catalytic ring opening of epoxides with carboxylic acids, Tetrahedron Lett. 38 (1997) 773–776, doi:10.1016/S0040-4039(96)02414-8.
[22] M.H. Wu, E.N. Jacobsen, An efficient formal synthesis of balanol via the asymmetric epoxide ring opening reaction, Tetrahedron Lett. 38 (1997) 1693–1696, doi:10.1016/S0040-4039(97)00192-5.
[23] S.E. Schaus, J. Brånalt, E.N. Jacobsen, Asymmetric hetero-Diels–Alder reactions catalyzed by chiral (Salen) Chromium(III) complexes, J. Org. Chem. 63 (1998) 403–405, doi:10.1021/jo971758c.
[24] F. Yang, J. Zhao, X. Tang, G. Zhou, W. Song, Q. Meng, Enantioselective α-hydroxylation by modified Salen-Zirconium(IV)-Catalyzed oxidation of β-Keto esters, Org. Lett. 19 (2017) 448–451, doi:10.1021/acs.orglett.6b03554.
[25] A. Naeimi, M. Honarmand, A. Sedri, Ultrasonic assisted fabrication of first MoO_3/copper complex bio-nanocomposite based on Sesbania sesban plant for green oxidation of alcohols, Ultrason. Sonochem. 50 (2019) 331–338, doi:10.1016/j.ultsonch.2018.09.037.
[26] O. Santoro, X. Zhang, C. Redshaw, Synthesis of biodegradable polymers: a review on the use of Schiff-base metal complexes as catalysts for the ring opening polymerization (ROP) of cyclic esters, Catalysts 10 (2020) 800, doi:10.3390/catal10070800.
[27] Y. Morimoto, S. Hanada, R. Kamada, A. Fukatsu, H. Sugimoto, S. Itoh, Hydroxylation of unactivated C (sp^3)–H bonds with m-chloroperbenzoic acid catalyzed by an Iron (III) complex supported by a trianionic planar tetradentate ligand, Inorg. Chem. 60 (2021) 7641–7649, doi:10.1021/acs.inorgchem.0c03469.
[28] S. De, A. Jain, P. Barman, Recent advances in the catalytic applications of chiral Schiff-base ligands and metal complexes in asymmetric organic transformations, ChemistrySelect 7 (2022) e202104334, doi:10.1002/slct.202104334.
[29] Y. Qin, H. Ren, F. Zhu, L. Zhang, C. Shang, Z. Wei, M. Luo, Preparation of POSS-based organic–inorganic hybrid mesoporous materials networks through Schiff base chemistry, Eur. Polym. J. 47 (2011) 853–860, doi:10.1016/j.eurpolymj.2011.02.024.
[30] J.L. Segura, M.J. Mancheño, F. Zamora, Covalent organic frameworks based on Schiff-base chemistry: synthesis, properties and potential applications, Chem. Soc. Rev. 45 (2016) 5635–5671, doi:10.1039/C5CS00878F.
[31] S. Xiong, Y. Wang, X. Wang, J. Chu, R. Zhang, M. Gong, B. Wu, Z. Li, Schiff base type conjugated organic framework nanofibers: solvothermal synthesis and electrochromic properties, Sol. Energy Mater. Sol. Cells 209 (2020) 110438, doi:10.1016/j.solmat.2020.110438.
[32] M. Nourmohammadi, S. Rouhani, S. Azizi, M. Maaza, T.A. Msagati, S. Rostamnia, M. Hatami, S. Khaksar, E. Zarenezhad, H.W. Jang, M. Shokouhimehr, Magnetic nanocomposite of crosslinked chitosan with 4, 6-diacetylresorcinol for gold immobilization (Fe_3O_4@ CS/DAR-Au) as a catalyst for an efficient one-pot synthesis of propargylamine, Mater. Today Commun. 29 (2021) 102798, doi:10.1016/j.mtcomm.2021.102798.
[33] C. Verma, M.A. Quraishi, Recent progresses in Schiff bases as aqueous phase corrosion inhibitors: design and applications, Coord. Chem. Rev. 446 (2021) 214105, doi:10.1016/j.ccr.2021.214105.
[34] C. Verma, M.A. Quraishi, A. Alfantazi, K.Y. Rhee, Corrosion inhibition potential of chitosan based Schiff bases: design, performance and applications, Intern, J. Biol. Macromol. 184 (2021) 135–143, doi:10.1016/j.ijbiomac.2021.06.049.
[35] M.T. Nguyen, B.J. Holliday, Direct insights into metal-induced conductivity enhancement in conducting metallopolymers, Chem. Commun. 51 (2015) 8610–8613, doi:10.1039/C5CC01719J.
[36] J. Zhang, L. Xu, W.Y. Wong, Energy materials based on metal Schiff base complexes, Coord. Chem. Rev. 355 (2018) 180–198, doi:10.1016/j.ccr.2017.08.007.
[37] F. Deng, X. Li, F. Ding, B. Niu, J. Li, Pseudocapacitive energy storage in Schiff Base polymer with Salphen-type ligands, J. Phys. Chem. C 122 (2018) 5325–5333, doi:10.1021/acs.jpcc.8b00434.
[38] L. Canali, D.C. Sherrington, Utilisation of homogeneous and supported chiral metal (salen) complexes in asymmetric catalysis, Chem. Soc. Rev. 28 (1999) 85–93, doi:10.1039/A806483K.
[39] E.M. McGarrigle, D.G. Gilheany, Chromium– and manganese– salen promoted epoxidation of alkenes, Chem. Rev. 105 (2005) 1563–1602, doi:10.1021/cr0306945.
[40] C.J. Whiteoak, G. Salassa, A.W. Kleij, Recent advances with π-conjugated salen systems, Chem. Soc. Rev. 41 (2012) 622–631, doi:10.1039/C1CS15170C.
[41] M.T. Kaczmarek, M. Zabiszak, M. Nowak, R. Jastrzab, Lanthanides: Schiff base complexes, applications in cancer diagnosis, therapy, and antibacterial activity, Coord. Chem. Rev. 370 (2018) 42–54, doi:10.1016/j.ccr.2018.05.012.
[42] S.T. Tsantis, D.I. Tzimopoulos, M. Holynska, S.P. Perlepes, Oligonuclear actinoid complexes with Schiff bases as ligands—older achievements and recent progress, Int. J. Mol. Sci. 21 (2020) 555, doi:10.3390/ijms21020555.
[43] J. Huang, J.C. Worch, A.P. Dove, O. Coulembier, Update and challenges in carbon dioxide-based polycarbonate synthesis, ChemSusChem 13 (2020) 469–487, doi:10.1002/cssc.201902719.
[44] Y.S. Wei, M. Zhang, R. Zou, Q. Xu, Metal–organic framework-based catalysts with single metal sites, Chem. Rev. 120 (2020) 12089–12174, doi:10.1021/acs.chemrev.9b00757.
[45] R. Mazzoni, F. Roncaglia, L. Rigamonti, When the metal makes the difference: template syntheses of tridentate and tetradentate salen-type Schiff base ligands and related complexes, Crystals 11 (2021) 483, doi:10.3390/cryst11050483.
[46] Y. Lin, H. Betts, S. Keller, K. Cariou, G. Gasser, Recent developments of metal-based compounds against fungal pathogens, Chem. Soc. Rev. 50 (2021) 10346–10402, doi:10.1039/D0CS00945H.
[47] M. Karmakar, S. Roy, S. Chattopadhyay, Synthesis, structure and properties of homo- and hetero-trinuclear complexes of salicylaldehyde-based di-Schiff bases, Polyhedron 215 (2022) 115652, doi:10.1016/j.poly.2022.115652.
[48] P. Das, W. Linert, Schiff base-derived homogeneous and heterogeneous palladium catalysts for the Suzuki–Miyaura reaction, Coord. Chem. Rev. 311 (2016) 1–23, doi:10.1016/j.ccr.2015.11.010.
[49] A. Erxleben, Transition metal salen complexes in bioinorganic and medicinal chemistry, Inorg. Chim. Acta 472 (2018) 40–57, doi:10.1016/j.ica.2017.06.060.
[50] M. Alighoivand, Z. Shaghaghi, R. Bikas, A. Kozakiewicz, Electrocatalytic water oxidation by a Ni(II) salophen-type complex, RSC Adv. 9 (2019) 40424–40436, doi:10.1039/C9RA08585H.
[51] S. Shaw, J.D. White, Asymmetric catalysis using chiral salen–metal complexes: recent advances, Chem. Rev. 119 (2019) 9381–9426, doi:10.1021/acs.chemrev.9b00074.
[52] S.H. Abbas, F. Adam, L. Muniandy, Green synthesis of MCM-41 from rice husk and its functionalization with nickel(II) salen complex for the rapid catalytic oxidation of benzyl alcohol, Microporous Mesoporous Mater. 305 (2020) 110192, doi:10.1016/j.micromeso.2020.110192.
[53] N. Aggarwal, S. Maji, Potential applicability of Schiff bases and their metal complexes during COVID-19 pandemic—a review, Rev. Inorg. Chem. (2022) De Gruyter, doi:10.1515/revic-2021-0027.
[54] Y.C. Yuan, M. Mellah, E. Schulz, O.R. David, Making chiral salen complexes work with organocatalysts, Chem. Rev. 122 (2022) 8841–8883, doi:10.1021/acs.chemrev.1c00912.
[55] M. Pervaiz, A. Sadiq, S. Sadiq, Z. Saeed, M. Imran, U. Younas, S.M. Bukhari, R.R.M. Khan, A. Rashid, A. Adnan, Design and synthesis of Schiff base Homobimetallic-Complexes as promising antimicrobial agents, Inorg. Chem. Commun. 137 (2022) 109206, doi:10.1016/j.inoche.2022.109206.
[56] P.G. Cozzi, Metal–Salen Schiff base complexes in catalysis: practical aspects, Chem. Soc. Rev. 33 (2004) 410–421, doi:10.1039/B307853C.
[57] A. Gualandi, F. Calogero, S. Potenti, P.G. Cozzi, Al (Salen) metal complexes in stereoselective catalysis, Molecules 24 (2019) 1716, doi:10.3390/molecules24091716.
[58] S.M. Elbert, M. Mastalerz, Metal salen-and salphen-containing organic polymers: synthesis and applications, Org. Mater. 2 (2020) 182–203, doi:10.1055/s-0040-1708501.
[59] B. Miroslaw, Homo- and hetero-oligonuclear Complexes of Platinum Group Metals (PGM) coordinated by imine Schiff base ligands, Int. J. Mol. Sci. 21 (2020) 3493, doi:10.3390/ijms21103493.
[60] Y. Zhang, P. Li, Y.J. Li, W.K. Dong, Exploring a more flexible N_2O_2-donor ligand and its octahedral tri-nuclear Co(II) and Ni(II) complexes, J. Coord. Chem. 74 (2021) 2017–2034, doi:10.1080/00958972.2021.1940981.
[61] R.M. Haak, S.J. Wezenberg, A.W. Kleij, Cooperative multimetallic catalysis using metallosalens, Chem. Commun. 46 (2010) 2713–2723, doi:10.1039/C001392G.
[62] M. Bazarnik, B. Bugenhagen, M. Elsebach, E. Sierda, A. Frank, M.H. Prosenc, R. Wiesendanger, Toward tailored all-spin molecular devices, Nano Lett. 16 (2016) 577–582, doi:10.1021/acs.nanolett.5b04266.
[63] Y. Sakata, C. Murata, S. Akine, Anion-capped metallohost allows extremely slow guest uptake and on-demand acceleration of guest exchange, Nat. Commun. 8 (2017) 1–7, doi:10.1038/ncomms16005.
[64] H. Houjou, Y. Hoga, Y.L. Ma, H. Achira, I. Yoshikawa, T. Mutai, K. Matsumara, Dinuclear fused salen complexes of group-10 metals: peculiarity of the crystal structure and near-infrared luminescence of a bis(Pt-salen) complex, Inorg. Chim. Acta 461 (2017) 27–34, doi:10.1016/j.ica.2017.01.031.
[65] J. Dong, Y. Liu, Y. Cui, Supramolecular chirality in metal–organic complexes, Acc. Chem. Res. 54 (2020) 194–206, doi:10.1021/acs.accounts.0c00604.
[66] D. Osypiuk, B. Cristóvão, L. Mazur, New heteronuclear complexes of PdII–LnIII–PdII with Schiff base ligand: synthesis, crystal structures and chemical properties, J. Mol. Struct. 1261 (2022) 132924, doi:10.1016/j.molstruc.2022.132924.
[67] I. Yoon, M. Goto, T. Shimizu, S.S. Lee, M. Asakawa, Synthesis and characterisation of macrocyclic palladium(II)–sodium(I) complexes: generation of an unusual metal-mediated electron delocalization, Dalton Trans. (2004) 1513–1515, doi:10.1039/B402507E.
[68] J. Gao, J.H. Reibenspies, R.A. Zingaro, F.R. Woolley, A.E. Martell, A. Clearfield, Novel chiral “calixsalen” macrocycle and chiral Robson-type macrocyclic complexes, Inorg. Chem. 44 (2005) 232–241, doi:10.1021/ic049181m.
[69] S. Akine, T. Nabeshima, Cyclic and acyclic oligo (N_2O_2) ligands for cooperative multi-metal complexation, J. Chem. Soc. Dalton Trans. (2009) 10395–10408, doi:10.1039/B910989G.
[70] S. Akine, M. Miyashita, S. Piao, T. Nabeshima, Perfect encapsulation of a guanidinium ion in a helical trinickel (II) metallocryptand for efficient reg-

ulation of the helix inversion rate, Inorg. Chem. Front. 1 (2014) 53–57, doi:10.1039/C3QI00067B.
[71] S. Akine, S. Piao, M. Miyashita, T. Nabeshima, Cage-like tris (salen)-type metallocryptand for cooperative guest recognition, Tetrahedron Lett. 54 (2013) 6541–6544, doi:10.1016/j.tetlet.2013.09.098.
[72] S. Akine, F. Utsuno, S. Piao, H. Orita, S. Tsuzuki, T. Nabeshima, Synthesis, ion recognition ability, and metal-assisted aggregation behavior of dinuclear metallohosts having a bis(saloph) macrocyclic ligand, Inorg. Chem. 55 (2016) 810–821, doi:10.1021/acs.inorgchem.5b02288.
[73] I. Mondal, S. Chattopadhyay, Development of multi-metallic complexes using metal-salen complexes as building blocks, J. Coord. Chem. 72 (2019) 3183–3209, doi:10.1080/00958972.2019.1695048.
[74] A.M. Madalan, N. Avarvari, M. Andruh, Metal complexes as second-sphere ligands, New J. Chem. 30 (2006) 521–523, doi:10.1039/B517989K.
[75] M. Mahato, D. Dey, S. Pal, S. Saha, A. Ghosh, K. Harms, H.P. Nayek, Syntheses, structures, optical properties and biological activities of bimetallic complexes, RSC Adv. 4 (2014) 64725–64730, doi:10.1039/C4RA11991F.
[76] M. Andruh, The exceptionally rich coordination chemistry generated by Schiff-base ligands derived from *o*-vanillin, Dalton Trans. 44 (2015) 16633–16653, doi:10.1039/C5DT02661J.
[77] Y. Zhang, W.X. Zhang, J.M. Zheng, Syntheses, structures, and properties of two dicyanamide-bridged polymers with a Schiff-base ligand, Z. Anorg. Allg. Chem. 642 (2016) 461–466, doi:10.1002/zaac.201600007.
[78] J.P. Costes, C. Duhayon, L. Vendier, A.J. Mota, Reactions of a series of ZnL, CuL and NiL Schiff base and non-Schiff base complexes with MCl_2 salts (M= Cu, Ni, Mn): syntheses, structures, magnetic properties and DFT calculations, New J. Chem. 42 (2018) 3683–3691, doi:10.1039/C7NJ04347C.
[79] S. Banerjee, A. Bauzá, A. Frontera, A. Saha, Exploration of unconventional π-hole and C–H···H–C types of supramolecular interactions in a trinuclear Cd(II) and a heteronuclear Cd (II)–Ni (II) complex and experimental evidence for preferential site selection of the ligand by 3d and 4d metal ions, RSC Adv. 6 (2016) 39376–39386, doi:10.1039/C6RA04428J.
[80] X. Gong, Y.Y. Ge, M. Fang, Z.G. Gu, S.R. Zheng, W.S. Li, S.J. Hu, S.B. Li, Y.P. Cai, Construction of four 3d-4d/4d complexes based on salen-type Schiff base ligands, Cryst. Eng. Commun. 13 (2011) 6911–6915, doi:10.1039/C1CE05525A.
[81] X.Z. Li, C.B. Tian, Q.F. Sun, Coordination-directed self-assembly of functional polynuclear lanthanide supramolecular architectures, Chem. Rev. 122 (2022) 6374–6458, doi:10.1021/acs.chemrev.1c00602.
[82] D. Visinescu, M.G. Alexandru, A.M. Madalan, C. Pichon, C. Duhayon, J.P. Sutter, M. Andruh, Magneto-structural variety of new 3d–4f–4(5)d heterotrimetallic complexes, Dalton Trans. 44 (2015) 16713–16727, doi:10.1039/C5DT01738F.
[83] I. Buta, S. Shova, S. Ilies, F. Manea, M. Andruh, O. Costisor, Mono- and oligonuclear complexes based on a o-vanillin derived Schiff-base ligand: synthesis, crystal structures, luminescent and electrochemical properties, J. Mol. Struct. 1248 (2022) 131439, doi:10.1016/j.molstruc.2021.131439.
[84] B. Miroslaw, B. Cristóvão, Z. Hnatejko, Structural, luminescent and thermal properties of heteronuclear PdII–LnIII–PdII complexes of hexadentate N2O4 Schiff base ligand, Molecules 23 (2018) 2423, doi:10.3390/molecules23102423.
[85] J.H. Lee, S.Y. Im, S.W. Lee, Pd–Ln and Pt–Ln complexes of a bi-compartmental ligand: $[MLn(L)(NO_3)_3]$ (M = Pd, Pt; Ln = Eu, Tb; H2L = N,N'-bis(3-methoxysalicylidenimino-1,3-diaminopropane)), Inorg. Chim. Acta 474 (2018) 89–95, doi:10.1016/j.ica.2018.01.020.
[86] J. Andrez, V. Guidal, R. Scopelliti, J. Pécaut, S. Gambarelli, M. Mazzanti, Ligand and metal based multielectron redox chemistry of cobalt supported by tetradentate Schiff bases, J. Am. Chem. Soc. 139 (2017) 8628–8638, doi:10.1021/jacs.7b03604.
[87] N. Mahlooji, M. Behzad, H. Amiri Rudbari, G. Bruno, B. Ghanbari, Unique examples of copper(II)/sodium(I) and nickel(II)/sodium(I) Schiff base complexes with bridging bis-bidentate Salen type ligand: synthesis, crystal structures and antibacterial studies, Inorg. Chim. Acta 445 (2016) 124–128, doi:10.1016/j.ica.2016.02.040.
[88] A. Finelli, N. Hérault, A. Crochet, K.M. Fromm, Threading Salen-type Cu- and Ni-complexes into one-dimensional coordination polymers: solution versus solid state and the size effect of the alkali metal ion, Cryst. Growth Des. 18 (2018) 1215–1226, doi:10.1021/acs.cgd.7b01769.
[89] D.F. Liu, X.Q. Lü, R. Lu, Homogeneous and heterogeneous styrene epoxidation catalyzed by copper (II) and nickel (II) Schiff base complexes, Transit. Metal Chem. 39 (2014) 705–712, doi:10.1007/s11243-014-9853-6.
[90] P.K. Bhaumik, A. Banerjee, T. Dutta, S. Chatterjee, A. Frontera, S. Chattopadhyay, Diminishing accessibility of electrophilic nickel(II) centres due to incorporation of a methylene spacer in the pendant side arm of a series of heterotrinuclear nickel (II)/sodium complexes: a DFT study using a homodesmotic equation, Cryst. Eng. Commun. 22 (2020) 2970–2977, doi:10.1039/D0CE90103B.
[91] X. Feng, K.Y. Wu, S.Y. Xie, R. Li, L. Wang, A heterometallic polymer based on bis-salicylidene Schiff base ligand, synthesis, electronic chemistry, and antibacterial property, Inorg. Nano-Metal Chem. 47 (2017) 1134–1140, doi:10.1080/24701556.2017.1284102.
[92] Y. Sui, D.P. Li, C.H. Li, X.H. Zhou, T. Wu, X.Z. You, Ionic ferroelectrics based on nickel Schiff base complexes, Inorg. Chem. 49 (2010) 1286–1288, doi:10.1021/ic902136f.
[93] X. Lü, W.-Y. Wong, W.-.K. Wong, Self-assembly of luminescent platinum-salen Schiff-base complexes, Eur. J. Inorg. Chem. (2008) 523–528, doi:10.1002/ejic.200700858.
[94] H.Y. Tsai, C.T. Ho, Y.K. Chen, Biological actions and molecular effects of resveratrol, pterostilbene, and 3′-hydroxypterostilbene, J. Food Drug Anal. 25 (2017) 134–147, doi:10.1016/j.jfda.2016.07.004.
[95] M.J.L. Fiego, A.S. Lorenzetti, G.F. Silbestri, C.E. Domini, The use of ultrasound in the South Cone region. Advances in organic and inorganic synthesis and in analytical methods, Ultrason. Sonochem. 80 (2021) 105834, doi:10.1016/j.ultsonch.2021.105834.
[96] Z. Li, T. Zhuang, J. Dong, L. Wang, J. Xia, H. Wang, X. Cui, Z. Wang, Sonochemical fabrication of inorganic nanoparticles for applications in catalysis, Ultrason. Sonochem. 71 (2021) 105384, doi:10.1016/j.ultsonch.2020.105384.
[97] M. Mittersteiner, F.F. Farias, H.G. Bonacorso, M.A. Martins, N. Zanatta, Ultrasound-assisted synthesis of pyrimidines and their fused derivatives: a review, Ultrason. Sonochem. 79 (2021) 105683, doi:10.1016/j.ultsonch.2021.105683.
[98] I.V. Machado, J.R. Dos Santos, M.A. Januario, A.G. Corrêa, Greener organic synthetic methods: sonochemistry and heterogeneous catalysis promoted multicomponent reaction, Ultrason. Sonochem. 78 (2021) 105704, doi:10.1016/j.ultsonch.2021.105704.
[99] S. Majhi, Applications of ultrasound in total synthesis of bioactive natural products: a promising green tool, Ultrason. Sonochem. 77 (2021) 105665.
[100] S.S. Low, M. Yew, C.N. Lim, W.S. Chai, L.E. Low, S. Manickam, B.T. Tey, P.L. Show, Sonoproduction of nanobiomaterials—a critical review, Ultrason. Sonochem. 82 (2022) 105887, doi:10.1016/j.ultsonch.2021.105887.
[101] M. Draye, G. Chatel, R. Duwald, Ultrasound for drug synthesis: a green approach, Pharmaceuticals 13 (2020) 23, doi:10.3390/ph13020023.
[102] F.S. Shirazi, K. Akhbari, Sonochemical procedures; the main synthetic method for synthesis of coinage metal ion supramolecular polymer nano structures, Ultrason. Sonochem. 31 (2016) 51–61, doi:10.1016/j.ultsonch.2015.12.003.
[103] M. Kamali, R. Dewil, L. Appels, T.M. Aminabhavi, Nanostructured materials via green sonochemical routes—sustainability aspects, Chemosphere 276 (2021) 130146, doi:10.1016/j.chemosphere.2021.130146.
[104] M.H. Islam, M.T. Paul, O.S. Burheim, B.G. Pollet, Recent developments in the sonoelectrochemical synthesis of nanomaterials, Ultrason. Sonochem. 59 (2019) 104711, doi:10.1016/j.ultsonch.2019.104711.
[105] J. Xu, K. Cui, T. Gong, J. Zhang, Z. Zhai, L. Hou, F.U. Zaman, C. Yuan, Ultrasonic-assisted synthesis of N-doped, multicolor carbon dots toward fluorescent inks, fluorescence sensors, and logic gate operations, Nanomaterials 12 (2022) 312, doi:10.3390/nano12030312.
[106] A. Gedanken, Using sonochemistry for the fabrication of nanomaterials, Ultrason. Sonochem. 11 (2004) 47–55, doi:10.1016/j.ultsonch.2004.01.037.
[107] S. Kimani, S. Chakraborty, I. Irene, J. de la Mare, A. Edkins, A. du Toit, B. Loos, A. Blanckenberg, A. Van Niekerk, L.V. Costa-Lotufo, K.N. ArulJothi, S. Mapolie, S. Prince, The palladacycle, BTC2, exhibits anti-breast cancer and breast cancer stem cell activity, Biochem. Pharm. 190 (2021) 114598, doi:10.1016/j.bcp.2021.114598.
[108] R. Czarnomysy, D. Radomska, O.K. Szewczyk, P. Roszczenko, K. Bielawski, Platinum and palladium complexes as promising sources for antitumor treatments, Int. J. Mol. Sci. 22 (2021) 8271–8300, doi:10.3390/ijms22158271.
[109] M. Vojtek, M.P.M. Marques, I.M.P.L.V.O. Ferreira, H. Mota-Filipe, C. Diniz, Anticancer activity of palladium-based complexes against triple-negative breast cancer, Drug Discov. Today 24 (2019) 1044–1058, doi:10.1016/j.drudis.2019.02.012.
[110] A. Garoufis, S.K. Hadjikakou, N. Hadjiliadis, Palladium coordination compounds as anti-viral, anti-fungal, anti-microbial and anti-tumor agents, Coord. Chem. Rev. 253 (2009) 1384–1397, doi:10.1016/j.ccr.2008.09.011.
[111] N.K. Sharma, R.K. Ameta, M. Singh, From synthesis to biological impact of Pd (II) complexes: synthesis, characterization, and antimicrobial and scavenging activity, Biochem. Res. Int. (2016) 4359375, doi:10.1155/2016/4359375.
[112] L. Heidari, M. Ghassemzadeh, D. Fenske, O. Fuhr, M. Saeidifar, F. Mohsenzadeh, Unprecedented palladium(II) complex containing dipodal 1,3,4-thiadiazole derivatives: synthesis, structure, and biological and thermal investigations, New J. Chem. 44 (2020) 16769–16775, doi:10.1039/D0NJ02918A.
[113] A. Goudarzi, M. Ghassemzadeh, M. Saeidifar, K. Aghapoor, F. Mohsenzadeh, B. Neumüller, In vitro cytotoxicity and antibacterial activity of $[Pd(AMTTO)(PPh_3)_2]$: a novel promising palladium(II) complex, New J. Chem. 46 (2022) 3026–3034, doi:10.1039/D1NJ05545C.
[114] S. Majhi, Applications of ultrasound in total synthesis of bioactive natural products: a promising green tool, Ultrason. Sonochem. 77 (2021) 105665, doi:10.1016/j.ultsonch.2021.105665.
[115] D.E. Crawford, Solvent-free sonochemistry: sonochemical organic synthesis in the absence of a liquid medium, Beilstein J. Org. Chem. 13 (2017) 1850–1856, doi:10.3762/bjoc.13.179.
[116] O.V. Dolomanov, L.J. Bourhis, R.J. Gildea, J.A.K. Howard, H. Puschmann, OLEX2: a complete structure solution, refinement and analysis program, J. Appl. Cryst. 42 (2009) 339–341, doi:10.1107/S0021889808042726.
[117] G.M. Sheldrick, SHELXT—integrated space-group and crystal-structure determination, Acta Cryst A71 (2015) 3–8, doi:10.1107/S2053273314026370.
[118] G.M. Sheldrick, Crystal structure refinement with SHELXL, Acta Cryst. C71 (2015) 3–8, doi:10.1107/S2053229614024218.
[119] L. Ding, Z. Chu, L. Chen, X. Lü, B. Yan, J. Song, D. Fan, F. Bao, Pd-Salen and Pd-Salan complexes: characterization and application in styrene polymerization, Inorg. Chem. Commun. 14 (2011) 573–577, doi:10.1016/j.inoche.2011.01.028.
[120] T.V. Basova, V.G. Kiselev, E.S. Filatov, L.A. Sheludyakova, I.K. Igumenov, Experimental and theoretical study of vibrational spectra of palladium (II) β-diketonates, Vib. Spectrosc. 61 (2012) 219–225, doi:10.1016/j.vibspec.2012.04.003.

[121] J.-C. Shi, T.-B. Wen, Y. Zheng, S.-J. Zhong, D.-X. Wu, Q.-T. Liu, B.-S. Kang, B.-M. Wu, T.C.W. Mak, Palladium complexes with simultaneous O:s coordination, syntheses, structures and characterization of complexes with 2-mercaptophenol or 2-mercaptopyridine N-oxide, Polyhedron 16 (1997) 369–375, doi:10.1016/0277-5387(96)00303-8.

[122] I. Yoon, M. Narita, T. Shimizu, M. Asakawa, Threading-followed-by-shrinking protocol for the synthesis of a [2]rotaxane incorporating a Pd (II)−salophen moiety, J. Am. Chem. Soc. 126 (2004) 16740–16741, doi:10.1021/ja0464490.

[123] D. Cunningham, P. McArdle, M. Mitchell, N.N. Chonchubhair, M. O'Gara, Adduct formation between alkali metal ions and divalent metal salicylaldimine complexes having methoxy substituents. A structural investigation, Inorg. Chem. 39 (2000) 1639–1649, doi:10.1021/ic990496p.

[124] P. Bhowmik, S. Chatterjee, S. Chattopadhyay, Heterometallic inorganic–organic frameworks of sodium–nickel (vanen): cation–π interaction, trigonal dodecahedral Na+ and unprecedented heptadentate coordination mode of vanen^{2-}, Polyhedron 63 (2013) 214–221, doi:10.1016/j.poly.2013.07.023.

[125] M. Das, S. Chatterjee, S. Chattopadhyay, Unique example of a trigonal dodecahedral Na^{+} in a compartmental Schiff base N,N′-(1, 2-Phenylene)-*bis* (3-methoxysalicylidene-imine), Inorg. Chem. Commun. 14 (2011) 1337–1340, doi:10.1016/j.inoche.2011.05.009.

[126] N. Wiberg, Lehrbuch der Anorganischen Chemie, 102. Auflage, de Gruyter, Berlin, New York., 2008, doi:10.1515/9783110206845.

[127] U. Holzwarth, N. Gibson, The Scherrer equation versus the 'Debye–Scherrer equation', Nat. Nanotechnol. 6 (2011) 534, doi:10.1038/nnano.2011.145.